AIAA JOURNAL
Vol. 44, No. 11, November 2006

Technical Notes

TECHNICAL NOTES are short manuscripts describing new developments or important results of a preliminary nature. These Notes should not exceed 2500 words (where a figure or table counts as 200 words). Following informal review by the Editors, they may be published within a few months of the date of receipt. Style requirements are the same as for regular contributions (see inside back cover).

Identification and Control of Three-Dimensional Separation on Low Swept Delta Wing

M. M. Yavuz and D. Rockwell
Lehigh University, Bethlehem, Pennsylvania 18015

DOI: 10.2514/1.24756

I. Introduction

RECENT interest in unmanned combat air vehicles (UCAVs) has stimulated investigation of the flow structure, as well as its control, on delta wings having low and moderate values of sweep angle. In addition, microair vehicles (MAVs) typically have complex leading-edge forms, including relatively low values of sweep angle. The distinctive features of the instantaneous and averaged flow structure on a delta wing of sweep angle $\Lambda = 50$ deg have been numerically computed by Gordnier and Visbal [1]. Taylor et al. [2] employed a dye technique, along with complementary particle image velocimetry, to visualize the vortex development on the moderately swept ($\Lambda = 50$ deg) wing, and Taylor and Gursul [3] investigated the near-surface topology and buffeting phenomena on the same planform. The foregoing investigations indicate that, at low angle of attack, a dual primary vortex system is established, whereas at higher angles of attack, this dual structure gives way to a single, larger-scale vortex. Ol and Gharib [4] employed a stereo version of particle image velocimetry to characterize the three-dimensional structure on crossflow planes of wings of sweep angle $\Lambda = 50$ deg and 65 deg. Honkan and Andreopoulos [5] determined patterns of instantaneous vorticity on a delta wing of sweep angle $\Lambda = 45$ deg via a pointwise technique and identified the existence of stationary discrete vortical structures, within the feeding sheet and the primary vortex.

Another possible form of leading-edge vortex, which occurs for a wing of sweep angle $\Lambda = 38.7$ deg, involves formation of an elongated vorticity layer that tends to reattach to the surface of the wing. This has been characterized by Yaniktepe and Rockwell [6] via particle image velocimetry (PIV). Yaniktepe and Rockwell [7] addressed the flow structure at the trailing-edge region on diamond and lambda planforms of a low swept wing. Yavuz et al. [8] investigated the near-surface topology and flow structure for a wing of sweep angle $\Lambda = 38.7$ deg, including the effect of wing perturbations and transient motion of the wing; a near-surface technique of PIV was employed. Yavuz and Rockwell [9] determined the near-surface flow patterns of a wing of sweep angle $\Lambda = 35$ deg and investigated the effect of trailing-edge control mechanism for various angles of attack. Such control can take the form of either one or more thrust vector systems, or localized control jets of a small cross-sectional area along the trailing edge. In the case of MAV configurations at low flight velocity, the velocity of the control jet, in a steady state or burst mode, may be relatively large.

The crossflow structure on delta wings of low sweep angle, in absence of a control technique, should be characterized with particular attention to the occurrence of vortex breakdown, or even loss of an identifiable vortex structure. These features should be interpreted in conjunction with the near-surface flow patterns. This approach can potentially lead to identification of three-dimensional separation from the surface of the wing, in relation to the existence or nonexistence of a leading-edge vortex.

Control at the trailing edge is known, from the investigation of Yavuz and Rockwell [9], to have a global effect on the near-surface flow structure of a wing of low sweep angle. The effect of this global influence on the flow structure in crossflow planes has not been addressed and should be determined in terms of patterns of mean and fluctuating parameters. The possibility of recovery of a highly ordered structure of the leading-edge vortex and a radical transformation of the form of the surface-normal fluctuations should be pursued. The latter has important consequences for buffet loading of the wing surface.

II. Experimental System and Techniques

Experiments were performed in a large-scale water channel, which had a test section of 927 mm width, 610 mm depth, and 4928 mm length. The walls of this section were optically transparent. The value of Reynolds number Re based on chord C was maintained at 10,000. The corresponding value of freestream velocity was $U_\infty = 96.8$ mm/s. The angle of attack of the wing was $\alpha = 8$ deg.

The delta wing had a sweep angle of $\Lambda = 35$ deg, a chord C of 98 mm, and a total span at the trailing edge of 280 mm. The thickness of the wing was 12.7 mm, and its leading edges were beveled on the windward side at an angle of 15 deg. The inside of the delta wing was machined in the form of a cavity, to allow the generation of uniform blowing from the trailing edge; this blowing is represented in the schematic of Fig. 1. For the jet system, the center of each slit was located 50.8 mm from the plane of symmetry of the wing. Each slit had a width of 25.4 mm and thickness of 0.8 mm. Seven different jet velocities were employed. These velocities corresponded to seven different momentum coefficients, $C_\mu = 0.006$, 0.025, 0.1, 0.23, 0.4, 0.92, and 1.63. To demonstrate the principal effects of trailing-edge blowing, addressed herein, the blowing coefficients $C_\mu = 0.1$, 0.4, and 1.63 are described, relative to the case of no blowing $C_\mu = 0$. The momentum coefficient was calculated as follows: $C_\mu = (V_j^2 \times A_j)/(U^2 \times A_s)$, in which V_j is the mean velocity of blowing at the trailing edge, A_j is the total area of both blowing slots at the trailing edge, A_s is the surface area of the planform, and U is the freestream velocity. The corresponding values of velocity ratio were $V_j/U = 5.8$, 11.6, and 23.5.

A technique of high-image-density particle image velocimetry was employed. Illumination was provided by a dual-pulsed Nd:Yag laser system, having a maximum output of 90 mJ. Twelve micron metallic coated particles were used for seeding. The laser sheet was located at $x/C = 0.34$ and 0.8, where x is measured from the tip of the apex and C is the chord length of the planform.

For the PIV technique, the images were recorded by a CCD camera and an effective framing rate of 15 cps was used. The pattern of instantaneous velocity vectors was obtained by a frame to frame cross-correlation technique involving successive frames of patterns

Received 22 April 2006; revision received 23 July 2006; accepted for publication 1 August 2006.

of particle images in an interrogation window 32×32 pixels. An effective overlap of 50% was employed, to satisfy the Nyquist criterion. The effective resolution, that is, grid size, was $\Delta/C = 0.0162$, and 0.0264, respectively, for the laser sheet locations at $x/C = 0.34$ and 0.8.

After the instantaneous velocity field V was determined, the time-averaged patterns of velocity $\langle V \rangle$, axial vorticity $\langle \omega \rangle$, streamlines $\langle \Psi \rangle$, and root-mean-square surface-normal velocity fluctuation w_{rms}/U were calculated by using the cinema sequence of images. Time-averaged patterns are based on 200 images of the instantaneous velocity field. Preliminary investigations to assess the rate of convergence as a function of the number of images indicated that convergence was essentially attained with 100 images. These patterns were interpreted in conjunction with the foregoing patterns of near-surface streamline patterns taken from Yavuz and Rockwell [9]; as a result, complementary representations of near-surface and crossflow streamline patterns were constructed.

The laser sheet locations for crossflow characterizations were based on the streamline patterns of the near-surface flow topology. A major consequence of trailing-edge blowing is that the large-scale swirl pattern associated with the focus is eradicated. This may be physically interpreted with the aid of previous investigations. Legendre [10], Perry and Hornung [11], Perry and Chong [12], Dallman and Schulte-Werning [13], Su et al. [14], Lazos [15], and Taylor and Gursul [3] showed an inward swirling surface streamline pattern which had a focus point in its center. This focus point was taken as an indicator of three-dimensional separation. The relationship between this focus at the surface and the flow away from the surface is the development of a three-dimensional vortical structure. To identify the effect of three-dimensional separation in conjunction with the steady trailing-edge blowing, a location slightly upstream of the focus of separation, $x/C = 0.34$, and a location further downstream of the focus of separation, $x/C = 0.8$, were selected.

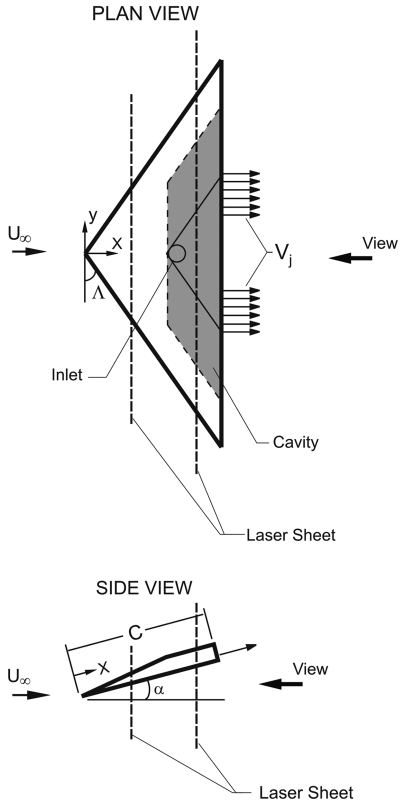

Fig. 1 Overview of experimental setup including delta wing and laser sheet orientation.

III. Time-Averaged Streamline Patterns

A. Time-Averaged Streamline Patterns in Crossflow Planes

Corresponding patterns of streamline topology of $\langle \psi \rangle$, based on the time-averaged velocity patterns (not shown here), are demonstrated in Fig. 2 for the values of blowing coefficients $C_\mu = 0$, 0.1, 0.4, and 1.63, and on the crossflow planes located at $x/C = 0.34$ and 0.8.

Consider patterns of $\langle \psi \rangle$ at $x/C = 0.34$ shown in the left column of images. In the absence of blowing $C_\mu = 0$, the streamlines appear to originate from a common node located close to the leading edge of the wing. Moreover, the overall pattern of $\langle \psi \rangle$ does not exhibit significant swirl. This distinctive form of the crossflow streamline pattern appears to be due to separation from the leading edge having relatively low sweep angle. It occurs in the presence of a highly separated flow in this region of the wing. Trailing-edge blowing at $C_\mu = 0.1$ induces a pronounced swirl of the streamlines. They spiral inward toward the focus, and therefore the focus is stable. Furthermore, at the larger values of $C_\mu = 0.4$ and 1.63, the inward spiral persists until a limit cycle is obtained. Within this limit cycle, the focus is associated with an outward spiraling streamline pattern, indicating that an unstable focus is embedded within the limit cycle. Viewing the patterns on the plane $x/C = 0.34$ as a whole, it is evident that increasing C_μ induces a detectable movement in the outboard direction of the focal point. Simultaneously, the overall swirl pattern of streamlines is displaced in the outboard direction. On the plane corresponding to $x/C = 0.8$, given in the right column of images, even for the case of no blowing, $C_\mu = 0$, a well-defined, inward-spiraling pattern of streamlines is evident. This general form of the spiral pattern, which terminates in a stable focus, persists for all values of blowing coefficient C_μ. The spanwise location of the focus, as well as the overall pattern of spiraling streamlines, is displaced substantially toward the leading edge for increasing C_μ. Furthermore, at larger values of C_μ, the swirling streamlines appear to coalesce together along the surface of the wing and remain parallel to the surface, before rolling up into the spiral pattern.

B. Comparison of Streamline Topology on Crossflow Planes and Along the Surface of the Wing

To further clarify the overall flow patterns, in relation to the magnitude of trailing-edge blowing, patterns of $\langle \psi \rangle$ in the crossflow planes and along the surface of the wing (Yavuz and Rockwell [9]) are superposed. These representations are given in Fig. 3 for $C_\mu = 0$ and 0.1, and in Fig. 4 for $C_\mu = 0.4$ and 1.63.

In Fig. 3, for $C_\mu = 0$, at $x/C = 0.34$, the relationship between the streamlines emanating from a node near the leading edge in the crossflow plane and the focus of the streamline pattern on the surface of the wing, associated with three-dimensional separation, is clearly evident. Further downstream, at $x/C = 0.8$, streamlines emanating from the leading edge are centered above the negative bifurcation line B_L^-. Streamlines associated with reattachment to the surface of the wing are centered approximately on the positive bifurcation line B_L^+. Furthermore, if the location of the focus (apparent center of the spiral streamline pattern) in the crossflow plane is projected onto the surface of the wing, that location corresponds to the location of turning of the surface streamlines, that is, the location at which they change direction from predominantly downstream- to upstream-oriented streamlines. By considering both of the planes at $x/C = 0.34$ and 0.8, the relationship between the focus at the surface and the flow away from the surface can be further defined. The development of the three-dimensional vortical structure due to the three-dimensional separation at the surface yields a well-defined swirling pattern at a location downstream of the focus of separation. It is evident that counterclockwise swirl of the separation region at the surface is associated with counterclockwise swirl in the crossflow plane. That is, the three-dimensional separation from the surface gives rise to a "vortex tube" that is deflected in the downstream direction, thereby appearing as the swirl pattern in the plane at $x/C = 0.8$. This concept is very similar to that obtained in the numerical simulation of Dallman and Schulte-Werning [13]. Their

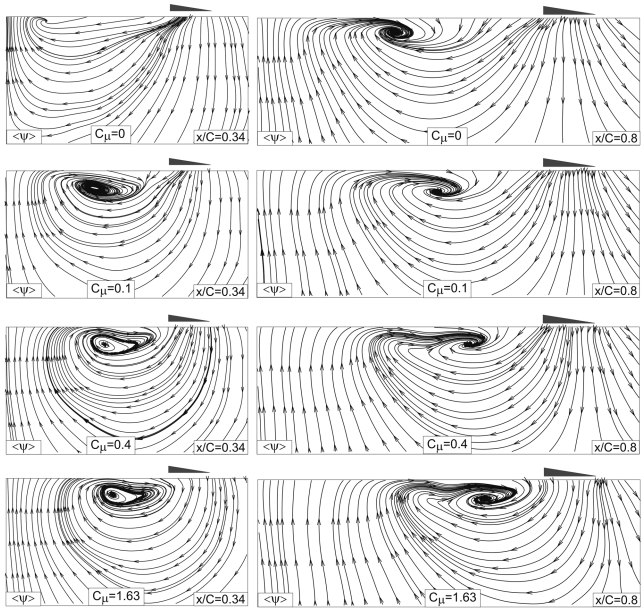

Fig. 2 Comparison of time-averaged streamline patterns for trailing-edge blowing at values of momentum coefficients $C_\mu = 0, 0.1, 0.4$, and 1.63 at the planes of interest $x/C = 0.34$ and 0.8.

representation shows that no swirl pattern is evident in the crossflow plane located upstream of the focus of separation, which is consistent with the present interpretation.

In general, the foregoing observations of the crossflow pattern of $\langle\psi\rangle$ at $x/C = 0.8$ for $C_\mu = 0$, relative to the corresponding pattern of $\langle\psi\rangle$ on the surface plane, hold for all values of the blowing coefficient, that is, for $C_\mu = 0.1$ in Fig. 3 and $C_\mu = 0.4$ and 1.63 in Fig. 4, irrespective of whether one considers the crossflow plane $x/C = 0.34$ or $x/C = 0.8$. That is, compatibility persists between 1) streamlines in the crossflow plane in the vicinity of the leading edge and the negative bifurcation line B_L^- on the surface plane; 2) streamlines associated with reattachment on the crossflow plane and the positive bifurcation line B_L^+ on the surface plane; and 3) the location of the focus on the crossflow plane in relation to the location

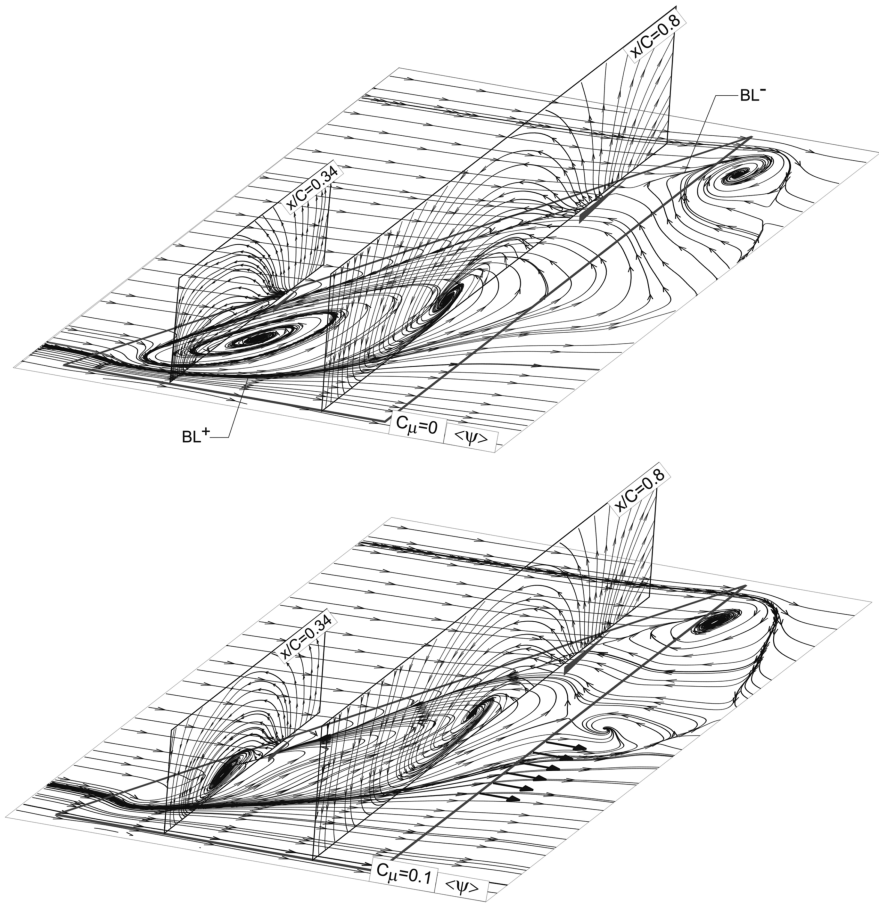

Fig. 3 Comparison of time-averaged near-surface streamline patterns with crossflow topology for trailing-edge blowing at values of momentum coefficients $C_\mu = 0$ and 0.1 at the planes of interest $x/C = 0.34$ and 0.8.

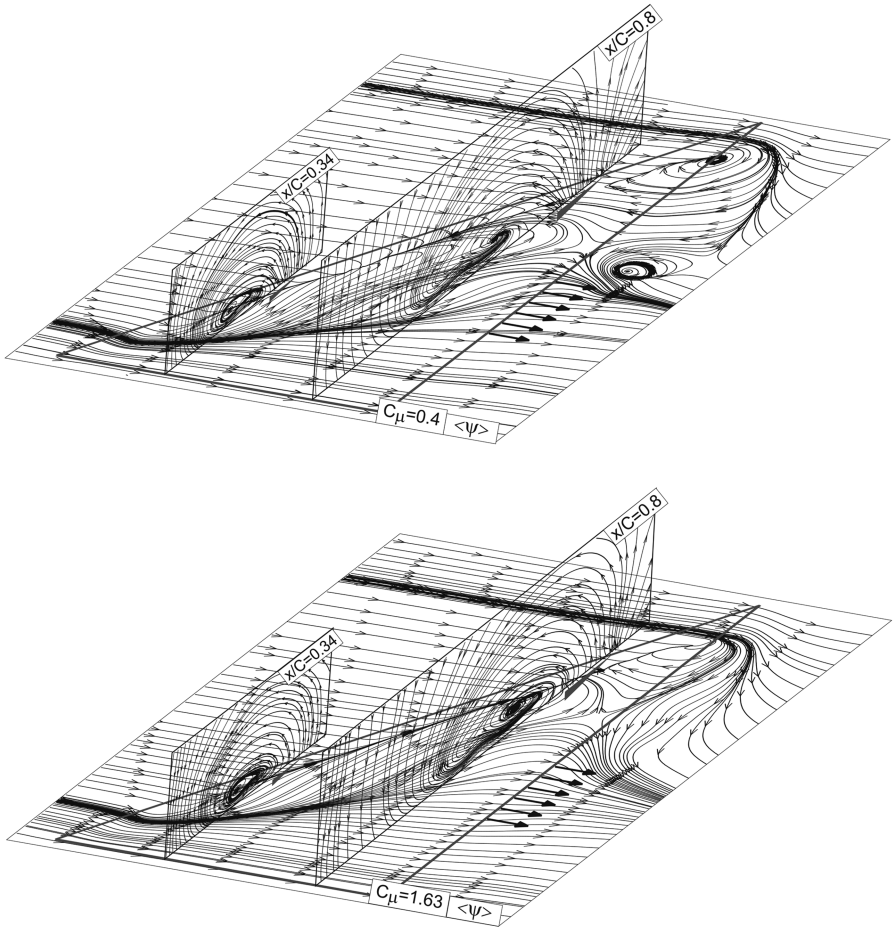

Fig. 4 Comparison of time-averaged near-surface streamline patterns with crossflow topology for trailing-edge blowing at values of momentum coefficients $C_\mu = 0.4$ and 1.63 at the planes of interest $x/C = 0.34$ and 0.8.

of turning of streamlines (from downstream to upstream orientation) on the surface plane.

Generally speaking, for increasing values of C_μ, the focus of the swirl patterns of streamlines in a crossflow plane, as well as the location of streamline turning in the surface patterns of streamlines, moves in the outward direction toward the leading edge.

IV. Patterns of Axial Vorticity

Contours of constant axial vorticity $\langle\omega\rangle$ are given in Fig. 5. Solid (dark) and dashed (light) lines represent, respectively, positive and negative contours of $\langle\omega\rangle$, in which the positive orientation corresponds to a vorticity vector in the direction of the outward normal vorticity vector, oriented in the streamwise direction. The left and right columns of images represent, respectively, planes at $x/C = 0.34$ and 0.8.

Consider the case of no blowing $C_\mu = 0$ in the first row of images. At $x/C = 0.34$, a concentration of $\langle\omega\rangle$ is located close to the plane of symmetry of the wing. As visualized by Yaniktepe and Rockwell [6], dye visualization shows that, at sufficiently high angle of attack, where large-scale separation/stall occurs on the surface of the wing the marker originating from the apex is close to the plane of symmetry of the wing. The indicated concentration of $\langle\omega\rangle$ is therefore indicative of the vorticity shed from the apex region. Furthermore, between this concentration of vorticity and the leading edge of the wing, low level, elongated contours of $\langle\omega\rangle$ are apparent, and there is no indication of a leading-edge vortex. At the leading edge, the small-scale concentration is associated with the rapid flow distortion in that region. At $x/C = 0.8$, the inboard concentration of vorticity is hypothesized to be an extension of the foregoing concentration at $x/C = 0.34$, whereas the outboard concentration most likely arises from the three-dimensional separation process from the wing surface.

In the presence of blowing, the patterns of vorticity at $x/C = 0.34$ represent a well-defined, leading-edge vortex(ices). At $C_\mu = 0.1$ and 0.4, a single concentration of vorticity is evident; it is part of an elongated vorticity layer. At $C_\mu = 1.63$, two identifiable concentrations of vorticity occur within the elongated layer. Furthermore, a pattern of positive $\langle\omega\rangle$ appears between the negative layer of $\langle\omega\rangle$ and the surface of the wing. It is due to eruption of the boundary layer from the wing surface. Finally, a common feature for all values of C_μ (at $x/C = 0.34$) is occurrence of a well-defined, small-scale concentration of vorticity at the leading edge; it is present even for the limiting case of no blowing $C_\mu = 0$. This concentration is associated with rapid distortion of flow from the leading edge.

At $x/C = 0.8$, in presence of blowing over the range $C_\mu = 0.1$ to 1.63, the pattern of negative $\langle\omega\rangle$ transforms from an elongated layer having a single concentration of vorticity to a layer having two concentrations of vorticity. This transformation is in parallel with the change in flow structure at $x/C = 0.34$ over the same range of C_μ. Moreover, an increase of C_μ results in an increase in magnitude of the peak vorticity, which occurs in the dominant, primary vortex structure. The second concentration of vorticity, of significantly lower magnitude, is, however, readily identifiable at $C_\mu = 0.4$ and 1.63. Furthermore, at larger values of C_μ, at $x/C = 0.8$, the positive concentration of vorticity adjacent to the wing surface is evident.

The existence of two concentrations of vorticity in the vorticity layer, as well as the positive concentration of vorticity adjacent to the surface of the wing, which occurs at the highest value of $C_\mu = 1.63$ and in both of the planes at $x/C = 0.34$ and 0.8, is remarkably similar to those first identified in the numerical simulation of Gordnier and Visbal [1] at lower angle of attack, and in the experimental observations of Taylor et al. [2], and Yaniktepe and Rockwell [6,7],

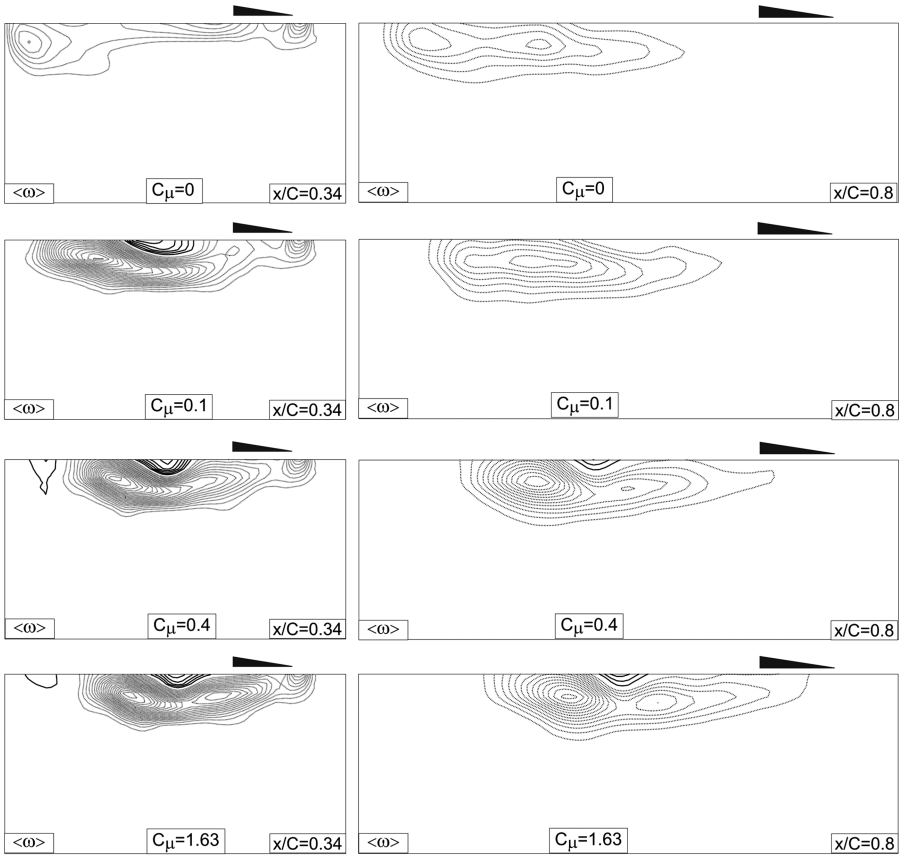

Fig. 5 Contours of constant axial vorticity $\langle\omega\rangle$ for trailing-edge blowing at values of momentum coefficients $C_\mu = 0$, 0.1, 0.4, and 1.63 at the planes of interest $x/C = 0.34$ and 0.8 ($[|\langle\omega\rangle|]_{\min} = 1\ \mathrm{s}^{-1}$, $\Delta[|\langle\omega\rangle|] = 1\ \mathrm{s}^{-1}$).

also at lower angle of attack, and in absence of blowing. We therefore conclude that highly separated flow along a wing of low sweep angle, which is present at moderate angle of attack, can be transformed to the dual vortex pattern, via localized control at the trailing edge (in the form of steady blowing). This dual vortex occurs naturally, that is, in absence of any control, at low angle of attack. Furthermore, this dual vortex exists over the entire streamwise extent of the wing.

Direct comparison of the vorticity contours on both planes of interest in presence of blowing shows significant reduction in the negative vorticity values in the plane further downstream, at $x/C = 0.8$. This reduction in the magnitude of negative vorticity at the downstream axial location may be due either to occurrence of vortex breakdown of the leading-edge vortices or the onset of unsteadiness due to the inherent instability of this system.

V. Patterns of Velocity Fluctuation

Contours of constant root-mean-square velocity fluctuation w_{rms}/U, defined in the direction normal to the surface of the wing, are given in Fig. 6. The layout of these patterns of w_{rms}/U is the same as those of $\langle\omega\rangle$ in Fig. 5. Surface-normal velocity fluctuations are directly related to the unsteady pressure at the surface of the wing, which is associated with unsteady loading, that is, buffeting, of the surface. The relationship between these velocity fluctuations and the buffet loading is addressed by Ozgoren et al. [16].

At $x/C = 0.34$, for the case of no blowing $C_\mu = 0$, which corresponds to a location immediately upstream of the focus F_2 of the large-scale separation from the surface of the wing, several isolated, low level clusters of w_{rms}/U are evident. On the other hand, at $x/C = 0.8$, for the case $C_\mu = 0$, significantly large values of w_{rms}/U are evident, and the pattern of contours extends over nearly the entire semispan of the wing. Comparison of these patterns for $C_\mu = 0$ at $x/C = 0.34$ and 0.8 therefore indicates that, at a location close to large-scale surface separation ($x/C = 0.34$), the fluctuation amplitude w_{rms}/U is relatively small, whereas well downstream of this onset of separation ($x/C = 0.8$), the fluctuation amplitudes are substantial and of large spatial extent.

The effects of trailing-edge blowing on the patterns of w_{rms}/U at $x/C = 0.34$, for successively larger values of $C_\mu = 0.1$, 0.4, and 0.163, are given in the left column of images of Fig. 6. The spanwise locations of the peak values of w_{rms}/U are approximately the same for different magnitudes of C_μ. On the other hand, the overall spatial extent of each pattern of w_{rms}/U becomes smaller, and the peak values larger, with increasing values of blowing coefficient C_μ. This transformation of patterns of w_{rms}/U can be directly compared with the corresponding patterns of vorticity concentrations $\langle\omega\rangle$ in Fig. 5. It corresponds to a change from a single vortex to a dual vortex structure within the elongated vorticity layer above the surface.

Further downstream, at $x/C = 0.8$, represented in the right column of images of Fig. 6, the effect of increasing C_μ is to increase the degree of concentration of the patterns of w_{rms}/U, and simultaneously, to decrease their overall spatial extent along the semispan of the wing. It should be noted, however, that the peak values of w_{rms}/U are approximately the same for all values of C_μ. In fact, for the largest value of $C_\mu = 1.63$, the pattern of w_{rms}/U covers less than half of the semispan, which indicates that only a limited extent of the wing surface is exposed to turbulent buffeting. Finally, the evolutions of these patterns of w_{rms}/U with increasing C_μ, when compared directly with the corresponding patterns of vorticity $\langle\omega\rangle$ in Fig. 5, indicate that the substantial decrease in spanwise extent of the pattern of w_{rms}/U corresponds to onset of the dual vortex structure, most evident at $C_\mu = 1.63$. Furthermore, it should be noted that these patterns of fluctuation are in accord with the patterns of transverse velocity fluctuation along the near-surface flow characterized by Yavuz and Rockwell [9]; that is, they occur at the same spanwise locations and have equivalent spatial extents.

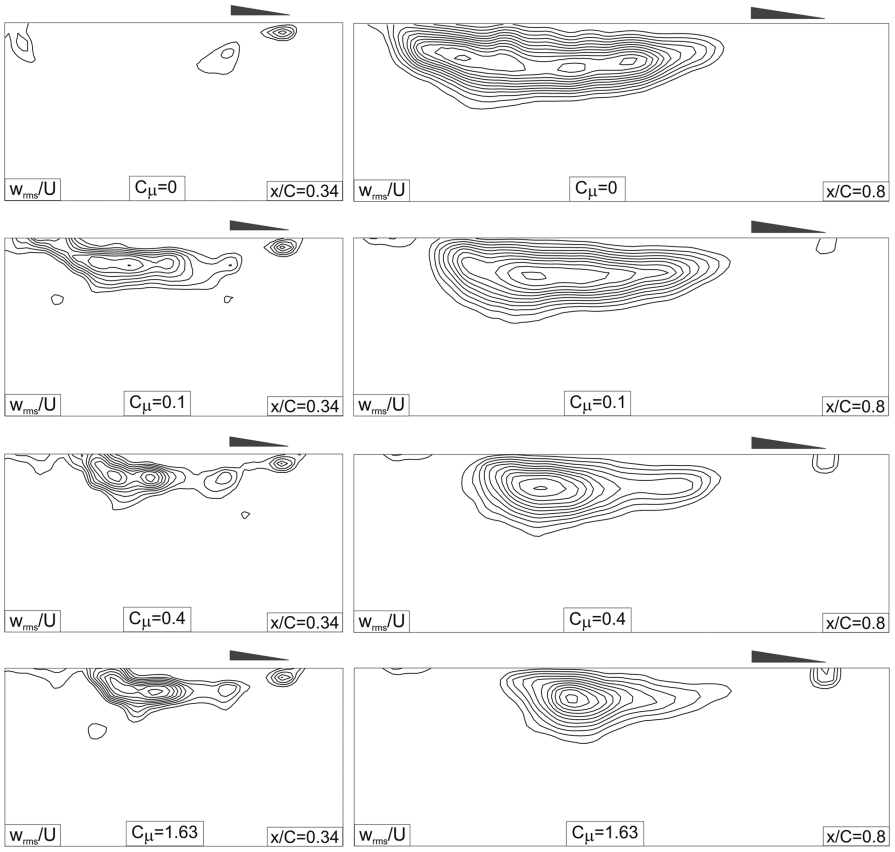

Fig. 6 Contours of constant root-mean-square normal velocity fluctuation w_{rms}/U for trailing-edge blowing at values of momentum coefficients $C_\mu = 0$, 0.1,0.4, and 1.63 at the planes of interest $x/C = 0.34$ and 0.8. ($[w_{\mathrm{rms}}/U]_{\mathrm{min}} = 0.04$, $\Delta[w_{\mathrm{rms}}/U] = 0.01$).

VI. Concluding Remarks

The flow structure on crossflow planes, located upstream and downstream of the onset of three-dimensional separation from the surface of a delta wing having low sweep angle, has been investigated as a function of the magnitude of localized blowing from slots at the trailing edge. The principal findings can be listed as follows:

1) In the absence of control, a region of three-dimensional separation dominates the near-surface flow, and the crossflow structure is characterized by the vortex shed from the apex and the three-dimensional vortex structure that emanates from three-dimensional separation from the surface. There is no indication of a leading-edge vortex.

2) Occurrence of three-dimensional separation/stall causes remarkable patterns of surface-normal velocity fluctuations in the region close to the trailing edge of the planform. These patterns are indicative of buffeting/unsteady loading.

3) In the presence of trailing-edge blowing, eradication of three-dimensional separation from the surface of the wing is associated with recovery of both the swirl pattern of streamlines and the pronounced axial vorticity concentration in the crossflow plane closest to the apex. Further increases of blowing coefficient cause the center of the vortex structure in the crossflow planes to move closer to the leading edge of the planform.

4) At sufficiently high blowing coefficients, a dual vortex structure occurs. It involves a secondary concentration of axially oriented vorticity, which has the same sign as, and is immediately adjacent to, the primary vortex. This structure is very similar in form to that originally identified at lower angle of attack in the numerical simulation of Gordnier and Visbal [1], and confirmed in the experimental investigations of Taylor et al. [2], and Yaniktepe and Rockwell [6,7]. In other words, the separated flow along a wing of low sweep angle, at moderate angle of attack, can be transformed, via steady trailing-edge blowing, to the dual primary vortex structure, which occurs naturally, that is, in the absence of any control, at low angle of attack.

5) An increase of blowing coefficient decreases the overall spatial extent of the pattern of surface-normal velocity fluctuations along the semispan of the wing, at locations close to the trailing edge. For the largest value of blowing coefficient, this pattern covers less than half of the semispan, which indicates that only a limited extent of the wing surface is exposed to turbulent buffeting/unsteady loading.

Acknowledgments

The support of the Air Force Office of Scientific Research under Grant No. F49620-02-1-0061 is gratefully acknowledged. This AFOSR program was monitored by John Schmisseur and Rhett Jefferies.

References

[1] Gordnier, R. E., and Visbal, M. R., "Higher-Order Compact Difference Scheme Applied to the Simulation of a Low Sweep Delta Wing Flow," AIAA Paper 2003-0620, Jan. 2003.

[2] Taylor, G. S., Schnorbus, T., and Gursul, I., "An Investigation of Vortex Flows over Low Sweep Delta Wings," AIAA Paper 2003-4021, June 2003.

[3] Taylor, G. S., and Gursul, I., "Unsteady Vortex Flows and Buffeting of a Low Sweep Delta Wing," AIAA Paper 2004-1066, Jan. 2004.

[4] Ol, M. V., and Gharib, M., "Leading-Edge Vortex Structure of Nonslender Delta Wings at Low Reynolds Number," *AIAA Journal*, Vol. 41, No. 1, 2003, pp. 16–26.

[5] Honkan, A., and Andreopoulos, J., "Instantaneous Three-Dimensional Vorticity Measurements in Vortical Flow over a Delta Wing," *AIAA Journal*, Vol. 35, No. 10, 1997, pp. 1612–1620.

[6] Yaniktepe, B., and Rockwell, D., "Flow Structure on a Delta Wing of Low Sweep Angle," *AIAA Journal*, Vol. 42, No. 3, 2004, pp. 513–523.

[7] Yaniktepe, B., and Rockwell, D., "Flow Structure on Diamond and Lambda Planforms: Trailing-Edge Region," *AIAA Journal*, Vol. 43, No. 7, 2005, pp. 1490–1500.
[8] Yavuz, M. M., Elkhoury, M., and Rockwell, D., "Near-Surface Topology and Flow Structure on a Delta Wing," *AIAA Journal*, Vol. 42, No. 2, 2004, pp. 332–340.
[9] Yavuz, M. M., and Rockwell, D., "Control of Flow Structure on Delta Wing with Steady Trailing-Edge Blowing," *AIAA Journal*, Vol. 44, No. 3, 2006, pp. 493–501.
[10] Legendre, R., "Lignes de Courent d'un Ecoulement Continu," *La Recherche Aérospatiale*, No. 105, 1965, pp. 3–9.
[11] Perry, A. E., and Hornung, H. G. "Some Aspects of Three-Dimensional Separation. Part 2. Vortex Skeletons," *Zeitschrift fur Flugwissenschaften und Weltraumforschung*, Vol. 8, 1984, pp. 155–160.
[12] Perry, A. E., and Chong, M. S., "A Description of Eddying Motions and Flow Patterns Using Critical-Point Concepts," *Annual Review of Fluid Mechanics*, Vol. 19, 1987, pp. 125–155.
[13] Dallman, U., and Schulte-Werning, B., "Topological Changes of Axisymmetric and Non-Axisymmetric Vortex Flows," *Topological Fluid Mechanics, Proceedings of the IUTAM Symposium*, edited by H. K. Moffat, and A. Tsinober, Cambridge Univ. Press, Cambridge, England, U.K., pp. 372–383.
[14] Su, W., Liu, M., and Liu, Z., "Topological Structures of Separated Flows About a Series of Sharp-Edged Delta Wings at Angles-of-Attack up to 90°," *Topological Fluid Mechanics, Proceedings of the IUTAM Symposium*, edited by H. K. Moffat, and A. Tsinober, Cambridge Univ. Press, Cambridge, England, U. K., pp. 395–407.
[15] Lazos, B., "Surface Topology on the Wheels of a Generic Four-Wheel Landing Gear," *AIAA Journal*, Vol. 40, No. 12, 2002, pp. 2402–2412.
[16] Ozgoren, M., Sahin, B., and Rockwell, D., "Vortex Breakdown from a Pitching Delta Wing Incident upon a Plate: Flow Structure as the Origin of Buffet Loading," *Journal of Fluids and Structures*, Vol. 16, No. 3, April 2002, pp. 295–316.

F. Coton
Associate Editor